European Polymer Journal 235 (2025) 114097

Contents lists available at ScienceDirect

European Polymer Journal

journal homepage: www.elsevier.com/locate/europolj

A robust, biocompatible scaffold for peripheral nerve regeneration: integration of PLLA nanofibers with a RGD-like poly(amidoamine) hydrogel

Sergio Sciré [a], Marica Bianchi [b], Marco Pensabene [c], Andrea Dorigato [b], Nicolò Mauro [a,*]

[a] Laboratory of Biocompatible Polymers and INSTM Unit, Department of "Scienze e Tecnologie Biologiche Chimiche e Farmaceutiche" STEBICEF, University of Palermo, Via Archirafi 32, 90123 Palermo, Italy
[b] University of Trento, Department of Industrial Engineering and INSTM Unit, Via Sommarive, 9 38123 Trento, Italy
[c] Pediatric Surgery Unit, Department of Health Promotion, Mother and Child Care (PROMISE), Internal Medicine and Medical Specialities, University of Palermo, Via Alfonso Giordano 3, 90127 Palermo, Italy

ARTICLE INFO

Keywords:
Poly(amidoamine)s
PLLA
Polyesters
Hydrogels
Scaffold
Nerve regeneration
Schwann cells
RGD peptide

ABSTRACT

This work reports on a nanocomposite scaffold (PLLA-AGMA1) designed to support Schwann cell growth and promote peripheral nerve regeneration. The system combines a poly(L-lactic acid) (PLLA) electrospun network, providing mechanical stability and suturability, with a polyamidoamine hydrogel (AGMA1) designed to mimic the extracellular matrix. AGMA1 was synthesized via polyaddition of agmatine with 2,2-bis-acrylamidoacetic acid, using a 25 % excess of acrylamide functions to enable UV-induced crosslinking without additional initiators. The reactive end groups formed covalent bonds with nitrogen plasma-activated PLLA nanofibers. Physicochemical analyses confirmed the formation of a uniform, hydrophilic network with high swelling capacity (75–80 %) and preserved structural integrity. The material exhibited stable thermo-mechanical behavior and could withstand suturing. It might be noticed that the maximum tensile strength of PLLA-AGMA1 was comparable to that peripheral nerves (0.6 vs 0.8 MPa, respectively). Degradation studies showed progressive degradation of AGMA1 over time, favoring cell infiltration. Human Schwann cells cultured on PLLA-AGMA1 displayed excellent viability, adhesion, and proliferation up to 9 days of incubation, supporting the scaffold's suitability for nerve repair. The fabrication process, comprising electrospinning, plasma treatment, and UV crosslinking without intermediate purification, was straightforward and scalable, highlighting the clinical potential of this robust, biocompatible scaffold for peripheral nerve regeneration.

1. Introduction

The regeneration of nerve tissues following peripheral nerve injury (PNI) remains a significant challenge in the field of medicine, primarily due to the limited regenerative capacity of neural cells and the complexity of the microenvironment required for successful repair [1,2]. Globally, millions of PNI cases are registered annually, often lead to sensory and motor impairments that necessitate therapeutic interventions [3]. In cases of nerve injuries, where the nerve gap exceeds 3 cm, auto-grafting is considered the gold standard, since it ensures good clinical and functional outcomes, allowing nerve regeneration [4]. Moreover, the auto-graft is a non-immunogenic tissue, thus avoiding immune response in the receiving site. However, this procedure is not free from complications, which may affect both the donor and recipient sites [4,5]. These issues could be overcome by the use of biocompatible nerve conduits which promote nerve regeneration [6]. Tissue engineering has emerged as a promising approach to address these challenges by creating biomimetic scaffolds that support axonal growth, cellular alignment, and the delivery or stimulation of neurotrophic factors [3,7–9]. Advancements in neural tissue engineering have focused on the development of tissue-engineered nerve grafts as alternatives to autologous nerve grafts. These scaffolds, composed of biocompatible materials, aim to provide a supportive framework for axonal regeneration while mitigating the limitations of donor site morbidity and insufficient tissue availability [10]. An interesting approach in scaffold design involves nanostructured and hydrogel-based materials, which have shown enhanced outcomes by simulating the extracellular matrix and promoting cell attachment and neurite extension [11–13]. The incorporation of cell adhesion molecules (CAMs) into neural scaffolds has shown potential in enhancing functional recovery and remyelination

* Corresponding author.
E-mail address: nicolo.mauro@unipa.it (N. Mauro).

https://doi.org/10.1016/j.eurpolymj.2025.114097
Received 8 April 2025; Received in revised form 6 June 2025; Accepted 23 June 2025
Available online 23 June 2025

processes [14]. A particularly interesting strategy in this context is the use of scaffolds functionalized with Arg-Gly-Asp (RGD) sequences, a fibronectin-derived motif known to facilitate cell adhesion and proliferation [15,16]. Recent studies have demonstrated the critical role of hydrogels, such as gelatin, in enhancing the biofunctionality of electrospun polyester-based scaffolds for soft tissue engineering, thus reinforcing the importance of integrating hydrogels with electrospun nanofibers to better mimic the extracellular matrix (ECM) for enhancing cell adhesion and proliferation [17,18]. Despite these advancements, complete recovery from PNI remains challenging, highlighting the necessity for biomaterials to achieve more successful repair.

Various poly(amidoamine) (PAA) hydrogels have previously been evaluated as cell culture substrates, demonstrating their ability to support adhesion for a range of cell types [19,20]. One such PAA, known as AGMA1, is synthesized by the aza-Michael polyaddition of 4-aminobutylguanidine sulfate (agmatine) to 2,2-bisacrylamidoacetic acid. This water-soluble amphoteric PAA features a repeating unit that resembles the RGD structure and can lead to biomimetic hydrogels able to promote cell adhesion and proliferation [21–23]. However, AGMA1 hydrogels suffer from poor mechanical properties (storage modulus, $G' < 10^4$ Pa), limiting robustness and surgical suturability, which preclude their real-world medical applications. By incorporating mineral fillers such as montmorillonite or electrospun PLLA-based fibers, it is possible to overcome this limitation, achieving elastic moduli more suitable for the stresses encountered in human tissues ($G' > 10^5$ Pa) as well as keeping the ability to support cell proliferation [21,22]. This enhancement makes AGMA1-based nanocomposite hydrogels potential scaffolds for regenerative medicine applications.

Here, we developed and characterized a biodegradable PLLA reinforced composite hydrogel, henceforth named PLLA-AGMA1, endowed with biocompatibility, cell adhesion capability and suitable mechanical properties for potential application in PNI regeneration. PLLA, a biodegradable and biocompatible polyester synthesized from eco-sustainable processes, was chosen due to its good mechanical properties and processability. It is highly crystalline, chemically stable, and it can keep their structural integrity and stiffness during tissue formation *in vivo* [24,25]. Moreover, the degradation of PLLA lead to L-lactic acid, which is non-toxic and well-tolerated by the human body. However, L-lactic acid lowers local pH, promoting inflammation, and hinders cell differentiation in scaffolds [24,25]. Besides, PLLA hydrophobicity limits cell adhesion of many cytotypes [26]. To enhance its bioactivity, PLLA scaffolds were fabricated via electrospinning and subsequently functionalized with an AGMA1 hydrogel via surface nitrogen plasma functionalization and UV crosslinking. This combination aimed to create a biomimetic environment that supports cell proliferation, axonal outgrowth, cell proliferation, and functional nerve regeneration. We assessed their structural, morphological, mechanical, and surface properties, as well as their cell proliferation ability toward human Schwann cells (SC), which play a pivotal role in axonal regrowth and repair. SC create pathways for regenerating axons by forming structures known as the bands of Büngner which orchestrate various processes essential for peripheral nerve regeneration, including axon guidance, debris clearance, trophic support, and remyelination. These serve as guidance channels, helping axons grow in the right direction. SC also produce neurotrophic factors such as nerve growth factor (NGF) and brain-derived neurotrophic factor (BDNF), which promote neuron survival and axonal growth [27–30]. We successfully developed a promising biomimetic nanocomposite hydrogel scaffold with enhanced suturability and optimal biological and mechanical properties, making it a good candidate for PNI regeneration. This advancement paves the way for future in vivo studies in view of potential clinical translation.

2. Experimental session

2.1. Materials

2,2-Bis-acrylamido acetic acid *(BAC,* 96.5 %*)* was synthesized in our laboratory as previously described [31,32], Poly(L-lactide acid) (PLLA, $\overline{M}_n = 129kDa$, $PD = 1.87$), dichloromethane (99.9 %, DCM), dimethylformamide (99.5 %, DMF), $LiOH{\cdot}H_2O$ (98.5 %), agmatine sulfate (97 %), hydrochloric acid (37 %), Dulbecco Modified Egle Medium (DMEM), fetal bovine serum (FBS), glutamine, penicillin (100 U ml^{-1}), streptomycin (100 μg mL^{-1}), amphotericin B, and Alamar Blue (AB) assay kit were purchesed from Sigma Aldrich Merck, Milan Italy, and used as received. Nitrogen (99.999 %) was purchased by Airliquid. hTERT ipn02.3 2λ, Human Schwann cells (HSC) were provided by ATCC for Scientific Research.

2.2. Preparation of the nanocomposite hydrogel scaffold (PLLA-AGMA1)

2.2.1. Electrospinning of the PLLA scaffold

1.3 g of PLLA were dissolved in DCM (8 ml) by gentle stirring. After that, 4 ml of DMF were added to have a DCM/DMF mixture 2:1. The solution was left under stirring overnight at room temperature. The electrospinning was performed the day after, and it has always been performed within five days from solution preparation to avoid solvent evaporation. The mixture was kept at around 4 °C before use. The solution was sprayed using a 5 ml syringe fitted with a 20-gauge needle. A rotating cylinder, 4 cm in diameter, was used as the collector. The electrospun scaffold were carefully cut longitudinally, unfolded, and gently taken out from the collector to form a mat measuring 12 × 4 cm. The spinning parameters used for the whole spinning process were: feed rate 1.2 mL, voltage 13 kV, volume 3 mL, needle to collector distance 15 cm, collector rotation speed 120 rpm, cleaning frequency 5 min.

2.2.2. Synthesis of acrylamide end-capped AGMA1 oligomers

AGMA1 oligomers were synthesized as reported elsewhere [22,33], but with some modifications. Briefly, 525.2 mg of $LiOH{\cdot}H_2O$ (12.5 mmol) were dissolved in 4.1 mL of MilliQ water under continuous stirring. BAC (2.5 g, 12.28 mmol) and agmatine sulfate (2.1 g, 9.21 mmol) were gradually added to reactive mixture under stirring. The reaction mixture was stirred for 48 h, resulting in the formation of a viscous and transparent slurry. To finalize the process, 5 mL of MilliQ water were added and 37 % HCl was slowly used to adjust the pH to 5.0. The resulting solution was paper filtered and subsequently freeze-dried. The final yield was approximately 98 % w w^{-1}.

2.2.3. Functionalization of the electrospun PLLA scaffold with AGMA1 hydrogels

The surface functionalization of electrospun PLLA fibers was carried out by using a non-equilibrium Diener Electronics Plasma-Surface-Technology reactor equipped with a glass chamber. The PLLA scaffold was placed inside the plasma chamber, where nitrogen plasma was produced under vacuum (0.01 mbar) with a power of 2.5 W (15 mL min^{-1}, 10 min). Plasma-treated PLLA scaffolds were then placed in a glass mold, consisting of two silanized glass plates, and impregnated with an AGMA1 solution (1.12 g mL^{-1}) [22]. The impregnated scaffold, was placed in a polymerization chamber and exposed to UV irradiation (Hg Helios quartz lamp $\lambda < 366$ nm) for 10 min. After gently detaching the composite scaffold from the glass plates, it was washed up several times alternating between ultrapure water, ethanol, and hydrochloric acid pH 4. Subsequently, samples were immersed in an acidic solution at pH 4, and stored at approximately 4 °C.

2.3. Chemical, morphological, and physicochemical characterization of the nanocomposite hydrogel scaffold (PLLA-AGMA1)

2.3.1. Scanning electron microscopy (SEM)

SEM analyses were conducted to investigate the microscopic morphology of both PLLA scaffolds and nanocomposite PLLA-AGMA1 surfaces. The measurements were conducted by a Phenom Pro X (AlfaTest) operating at 10 kV and at different magnifications (1500x and 3700x) to highlight microstructural details. Each sample was sputtered with gold nanoparticles before performing acquisitions. The acquired SEM images were processed using ImageJ software to determine the average dimensional distribution of fibers, based on the measurement of 130 individual fibers. Results were expressed as mean ± standard deviation (SD), providing quantitative insights into the morphological variations across different sample types.

2.3.2. Attenuated total reflection Fourier transform infrared spectroscopy (FTIR-ATR) analysis

FTIR-ATR analyses of the bare scaffolds and the nanocomposite were performed using an FTIR spectrometer equipped with an ATR (Bruker, ALPHA, platinum-ATR), recording spectra within a range of 500 to 4000 cm^{-1} (16 scans, resolution of 4 cm^{-1}).

2.3.3. Contact angle measurements

Contact angle measurements were performed at ambient temperature and humidity on composite discs with a diameter of 8 mm. Water droplets (20 μL) were deposited on the composite surface and observed for approximately 1 min. Side profiles of the droplets were captured every 5 s and subsequently analyzed. Measurements were conducted on four separate samples, and the results were reported as the mean ± standard deviation.

2.3.4. Evaluation of the swelling behavior

The swelling degree of the composites was evaluated in three different solvents: MilliQ water, in aqueous solution at pH 5, and ethanol. Three samples were used for each solvent. The dry composites were immersed in the respective swelling media for approximately 1 h. They were then blotted, weighed, dried in a desiccator, and reweighed until a constant weight was achieved. Swelling was calculated using the Eq. (1):

$$SW(\%) = \frac{W_W - W_D}{W_D} \bullet 100 \quad (1)$$

Where W_D is the weight of the dry sample and W_w is the weight of the swollen sample. The results were reported as the mean values.

2.3.5. Determination of the degradation kinetics

The degradation rate of the composite PLAA-AGMA1 was evaluated by measuring the weight loss of samples in DPBS (Dulbecco's Phosphate Buffer Saline) at pH 7.4 and 37 °C. Samples were immersed in the medium and maintained in an orbital shaker (100 rpm) for four months. At established time intervals (2, 5, 7, 9, and 12 days), three samples were rinsed thoroughly with water, dried, and weighed again. The percentage weight loss ($W_l(\%)$) was calculated using the Eq. (2) [20]:

$$W_l(\%) = \frac{W_0 - W_f}{W_0} \bullet 100 \quad (2)$$

where W_0 is the initial dry weight of the disc, and W_f is the final dry weight of the disc.

2.4. Thermo-mechanical, mechanical and rheological characterization of the PLLA-AGMA1 nanocomposite scaffolds

2.4.1. Suturability assay

The suturability test simulated the entire procedure as closely as possible to clinical practice. The PLLA-AGMA1 sample was kept in an environment with 60 % relative humidity until testing. The same surgeon performed all incisions and sutures on the material within the same work session, using micro-scissors, appropriate microsurgical instruments, and 3x optical magnification, as is commonly used for microsurgical procedures. The PLLA-AGMA1 was transected full-thickness with micro-scissors along a single incision. The two stumps were then realigned to restore the same orientation and sutured with two separate simple 8–0 nylon 6,6 full-thickness stitches for each sample. The same procedure was performed by the same surgeon on control samples as well. Afterward, the sutured samples and controls were placed in the same container at 60 % relative humidity and stored at 4 °C before mechanical analyses were performed.

2.4.2. Thermal characterization

To investigate the degradation resistance of the electrospun PLLA, the AGMA hydrogel and the PLLA-AGMA composite, thermogravimetric analysis (TGA) was performed by using a Mettler TG50 thermo-balance (Mettler-Toledo GmbH, Schwerzenbach, Switzerland). Samples, with a weight of 20 mg each, were tested at a heating rate of 10 °C min^{-1} from 25 °C up to 700 °C under a nitrogen flow of 10 mL min^{-1}. The temperature associated with a mass loss of 5 % ($T_{5\%}$) and the residual mass at 200 °C, 500 °C and 700 °C (m_{200}, m_{500}, m_{700}) were respectively evaluated. Additionally, the temperatures corresponding to the maximum mass loss rate associated with water evaporation ($T_{H2O,peak}$), PLLA degradation ($T_{PLLA,peak}$), and the degradation steps of the hydrogel (T_{1peak}, T_{2peak}, T_{3peak}) were determined from the first derivative of the thermogravimetric curves (DTG). One specimen was tested for each formulation.

Differential scanning calorimetry (DSC) tests were performed on the PLLA electrospun mat, the AGMA hydrogel and the PLLA-AGMA composite by means of a Mettler DSC30 calorimeter (Mettler Toledo GmbH, Schwerzenbach, Switzerland). Measurements were carried out under 100 mL/min nitrogen flow between −50 °C and 200 °C, at a heating/cooling rate of 10 °C/min. The specimens, weighting approx. 10 mg, were subjected to a first heating scan, cooling scan and second heating scan. DSC analysis allowed the determination of the glass transition temperature (T_g) and the melting and cold crystallization temperatures (T_m, T_{cc}) of PLLA. The specific melting and cold crystallization enthalpy values (ΔH_m, ΔH_{cc}) of electrospun PLLA were also determined. Furthermore, the crystallinity degree (χ_c) of PLLA was calculated according to equation (3)

$$\chi(\%) = \frac{\Delta H_m - \Delta H_{cc}}{\Delta H_{0m}} \cdot 100 \quad (3)$$

where ΔH_{0m} is the theoretical melting enthalpy of fully crystalline PLLA, taken as 93 J g^{-1} (1). One specimen was tested for each formulation.

Dynamical mechanical analysis of the PLLA scaffold and the PLLA-AGMA composite was performed by using a DMA Q800 machine (TA instrument, New Castle, DE, USA) in tensile mode. Temperature ramp tests were carried out to investigate the dependence of storage modulus (E'), loss modulus (E'') and loss tangent (tanδ) on temperature. The tests were performed with a frequency of 1 Hz, a strain amplitude of 0.05 % and a heating ramp of 3 °C min^{-1} in a temperature interval from 25 to 120 °C. Rectangular specimens (gauge length 10 mm, width 5 mm, thickness 0.3 mm) were used, and one specimen was tested for each sample.

2.4.3. Mechanical characterization

Uniaxial tensile tests were performed to investigate the mechanical properties of the produced PLLA-AGMA composite and compare them with those of the electrospun PLLA. The tensile properties of the materials were evaluated using an Instron 5969 (Instron®, Norwood, MA, USA) tensile testing machine, equipped with a load cell of 100 N and operating at a cross-head speed of 5 mm min^{-1}. Tests were performed at

22 °C and RH = 50 % on rectangular specimens (gauge length 15 mm, width 5 mm, thickness 0.3 mm). For each type of material, five specimens were tested. The maximum stress (σ_{max}) and the strain at break (ε_{break}) were determined. By using the same testing conditions, uniaxial tensile tests were performed also on the sutured PLLA electrospun mat and PLLA-AGMA1 composite.

2.5. Biological characterization of the nanocomposite hydrogel scaffold (PLLA-AGMA1)

2.5.1. Cell culturing

Cell adhesion and proliferation assays were carried out using the hTERT ipn02.3 2λ, Human Schwann cells (HSC), a type of glial cell that surrounds neurons, keeping them alive, they are the major glial cell type in the peripheral nervous system. Cells were grown in DMEM containing 10 % FBS, 4 mM glutamine, and 100 U mL^{-1} —100 μg mL^{-1} penicillin–streptomycin (complete DMEM).

A 75 cm^2 flask containing log growing HSC was observed under an inverted fluorescence microscope (by Zeiss), equipped with a 5 × magnification objective. Micrographs were captured with an Axio Cam MRm (Zeiss) camera. The complete DMEM media was then removed, and cells were rinsed for a few minutes with PBS. The buffer solution was removed, and cells were incubated with 1 mL of trypsin/EDTA solution at 37 °C in 5 % CO_2 incubator for 5 min or until the monolayer started to detach from the flask. Cells were suspended in 5 mL of complete DMEM media and then were centrifuged at 700 *g* for 5 min. The pellet was suspended in an appropriate volume of DMEM and platted at a split ratio of 1:5 or 1:8 in a new 75 cm^2 flask.

2.5.2. Evaluation of the cell adhesion and proliferation

To evaluate the biocompatibility and the efficacy as substate for cell adhesion of PLLA-PAA composite scaffold, alamarBlue (AB) assay was used. HSC were seeded at a density of 8000 cells, directly in 6 mm dishes samples in 150 μl of DMEM in a 96 wells plate, then AB assay was carried out according to manufacturer's instructions. Briefly, medium was removed; cells were rinsed with PBS and 180 μl of an 10 % (v v^{-1}) AB solution prepared in fresh medium, without FBS or supplements, were added to each well. Following 3 h incubation, AB fluorescence was measured, at the respective excitation and emission wavelength of 530 and 590 nm, using an Eppendorf AF2200 microplate reader. Cells were tested after 1, 2, 5, 7 and 9 days. Cells seeded in untreated wells were used as positive control at each time interval. The results were averaged over 3 replicates per experiment reporting standard deviation and they were expressed as a percentage of the emission obtained from the AB solution placed directly in the well without any scaffold. For each experiment, wells containing only the AB solution without cells were also prepared and treated as samples. The fluorescence measured in those was used as a background and subtracted.

For routine culturing and qualitative evaluation of morphology, cells were analyzed under an Axio Vert.A1 FL-LED Inverted Microscope by Zeiss as above described.

2.6. Statistical data analysis

Statistical analysis was carried out using Student's T-test (two-tailed) for comparing two groups, and one-way analysis of variance (ANOVA) followed by Tukey's post-hoc analysis for comparing sets of data composed by multiple groups. Statistical calculations were performed using the Microsoft®-Excel data analysis tool and the software package GraphPad Prism (V.7.03). Comparisons were considered statistically significant at $p < 0.05$ (*), $p < 0.01$ (**), $p < 0.001$ (***), and $p < 0.0001$ (****).

3. Results and discussion

3.1. PLLA-AGMA1 nanocomposite hydrogel scaffold preparation

Previous investigations have demonstrated that PAAs derived from the Michael-type polyaddition of 2,2-biscrylamidoacetic acid (BAC) and agmatine sulfate represent a promising class of hydrogels for 3D cell cultivation [19,21,22,34]. These hydrogels can be obtained by covalent crosslinking using both ethylene diamine (or similar multifunctional molecules – mobile hydrogens > 3) as tetrafunctional Michael donor crosslinker or by UV radical crosslinking. The latter usually lead to robust biodegradable hydrogels whose average crosslinking degree can be easily controlled as a function of the molecular weight distribution of acrylamide end-capped AGMA1 oligomers (Scheme 1). For instance, AGMA1 oligomers obtained with 10 % ($\overline{DP}n = 19$) or 20 % ($\overline{DP}n = 9$) excess acrylamide, and crosslinked by UV irradiation in the presence of 4,4′-Azobis(4-cyanovaleric) acid as radical initiator, yield hydrogels with elastic modulus of 1 and 1.5 MPa, respectively [22]. The resulting material, referred to as AGMA1, exhibits several advantageous regenerative properties, including ease of preparation, controlled biodegradation via β-aminolysis, high cell biocompatibility, and enhanced adhesion due to its RGD-like structure [15,21,23].

To produce AGMA1 oligomers suitable to prepare hydrogels with higher stiffness we adopted the same procedure but using an excess acrylamide function of 25 % mol mol^{-1} suitable to obtain AGMA1 oligomers of $\overline{DP}n = 7$ (Scheme 1). For the preparation of the AGMA1 oligomers, lithium hydroxide.

was used to selectively deprotonate the primary amine group of agmatine in order to avoid crosslinking. Indeed, agmatine contains a primary amine group and a guanidine group, providing five hydrogen atoms potentially capable of participating in the polyaddition reaction. The amine and guanidine groups of agmatine differ significantly in basicity; the guanidine group has a pK_a of 12.5, which is considerably higher than that of typical aliphatic amines and remains protonated under the PAA synthetic conditions described in this study [35]. The addition of one mole of lithium hydroxide selectively deprotonates the amine group, yielding agmatine with a protonated guanidine residue that is unable to participate in the polyaddition process. The absence of crosslinking results in the formation of linear, soluble agmatine-based PAAs. An excess of approximately 25 % of double bonds, introduced by molar excess of BAC, allows the formation of oligomers with terminal acrylamide residues. ^{1}H NMR and SEC analyses showed the effective formation of oligomers with $\overline{M}_n$ of 2200 (PD = 1.75, $\overline{DP}n = 7$) bearing acrylamide end chains.

The acrylamide end chains can react with nucleophilic groups, such as amino groups, and contextually leading to gelation under UV irradiation. This approach has been harnessed to produce AGMA1 hydrogels reinforced with NH_2-functionalized PLLA nanofibers directly linked to the AGMA1 polymer network via Michael polyaddition, resulting in nanocomposite biodegradable scaffolds. These scaffolds integrate the biomimetic and cell-adhesion properties of AGMA1 hydrogels with the mechanical robustness of PLLA nanofibers, proving capable of supporting Human Pluripotent Stem Cell adhesion and proliferation up to 7 days [22]. For this reasons, PLLA electrospun scaffolds were prepared and functionalized with amino groups via plasma surface activation as described in our previous study [36,37], enabling subsequent AGMA1 grafting via amine functions and contextual UV crosslinking of residual double bonds by irradiation (Scheme 2).

The preparation of the nanocomposite PLLA-AGMA1 involves four distinct steps: (i) electrospinning to produce PLLA scaffolds, (ii) non-equilibrium nitrogen plasma surface activation of PLLA nanofibers to generate NH_2-PLLA, (iii) synthesis of AGMA1 oligomers with a controlled average molecular weight distribution, and (iv) fabrication of the nanocomposite through selective polyaddition between the primary amines of NH_2-PLLA fibers and the double bonds of acrylamide end-

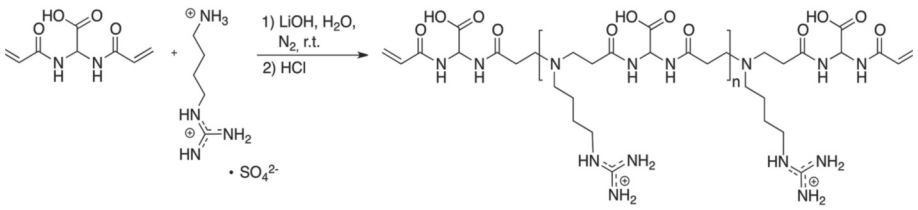

Scheme 1. Synthesis of AGMA1 oligomers adopted for the preparation of the nanocomposite hydrogel scaffold PLLA-AGMA1.

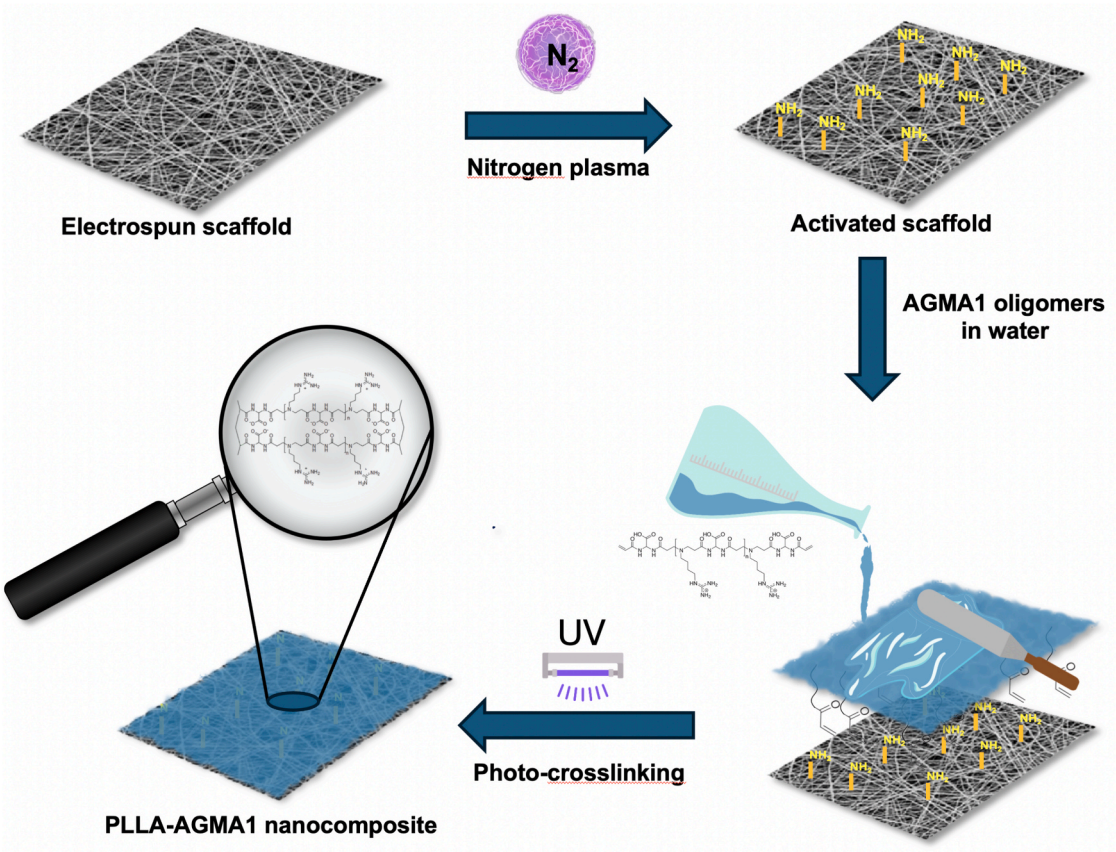

Scheme 2. Schematic representation of the synthetic pathway utilized for the synthesis of the nanocomposite PLLA-AGMA1 hydrogel scaffold.

capped AGMA1 oligomers, coupled with UV radical crosslinking without the addition of initiators. The production process is highly scalable due to its streamlined purification steps and the simplicity of technologies like electrospinning, PLLA plasma treatments, and UV irradiation. A major advantage is the direct use of AGMA1 oligomers without purification, reducing processing time and costs. Additionally, radical crosslinking occurs under UV light without initiators, simplifying formulation and ensuring biocompatibility. Purification was uniquely performed post-gelation via solvent extraction, transitioning from ethanol to water at pH 4. This efficient process removes unreacted monomers while preserving hydrogel integrity. These features make the method well-suited for industrial-scale production, particularly in biomedical applications requiring reproducibility and biocompatibility.

3.2. Morphological, chemical, and Physico-chemical Characterization of nanocomposite hydrogel scaffold (PLLA-AGMA1)

3.2.1. Scanning electron microscopy (SEM)

The morphology of the electrospun PLLA scaffold, before and after the plasma treatment, was studied by SEM microscopy (Fig. 1A-B). The bare scaffold consists of fibers of 495 ± 110 nm in radius anisotropically distributed (Fig. 1A and 1C) which confers huge porosity desired for cell infiltration and colonization. Nitrogen plasma, typically employed for NH_2 surface functionalization of polyesters, does not significantly alter the size distribution and morphology of PLLA nanofibers (Fig. 1B), suggesting that activated PLLA scaffolds are still suitable for the preparation of nanocomposite functionalized biomaterials. Although some additional bead-like structures are visible in the SEM micrograph after the plasma treatment (Fig. 1B), these are not a consequence of the plasma treatment but rather stem from the electrospinning process itself and the highly localized nature of SEM imaging, which may emphasize minor morphological features that are not representative of the overall scaffold structure. This is because the plasma treatment modifies the chemical bonds on the surface but does not alter the morphological structure of the material. In contrast, the SEM micrograph of the PLLA-AGMA1 composite (Fig. 1 D) shows that its surface presents a uniform and continuous layer of hydrogel, confirming that the AGMA1 hydrogel network has entirely coated the electrospun structure, saturating the scaffold porosity and making the surface smooth. This is also confirmed by the SEM micrograph of the PLLA-AGMA1 cross-section (insert, Fig. 1D), where it is clearly visible that the AGMA1 network penetrates throughout the scaffold and each fiber is overwhelmed with the

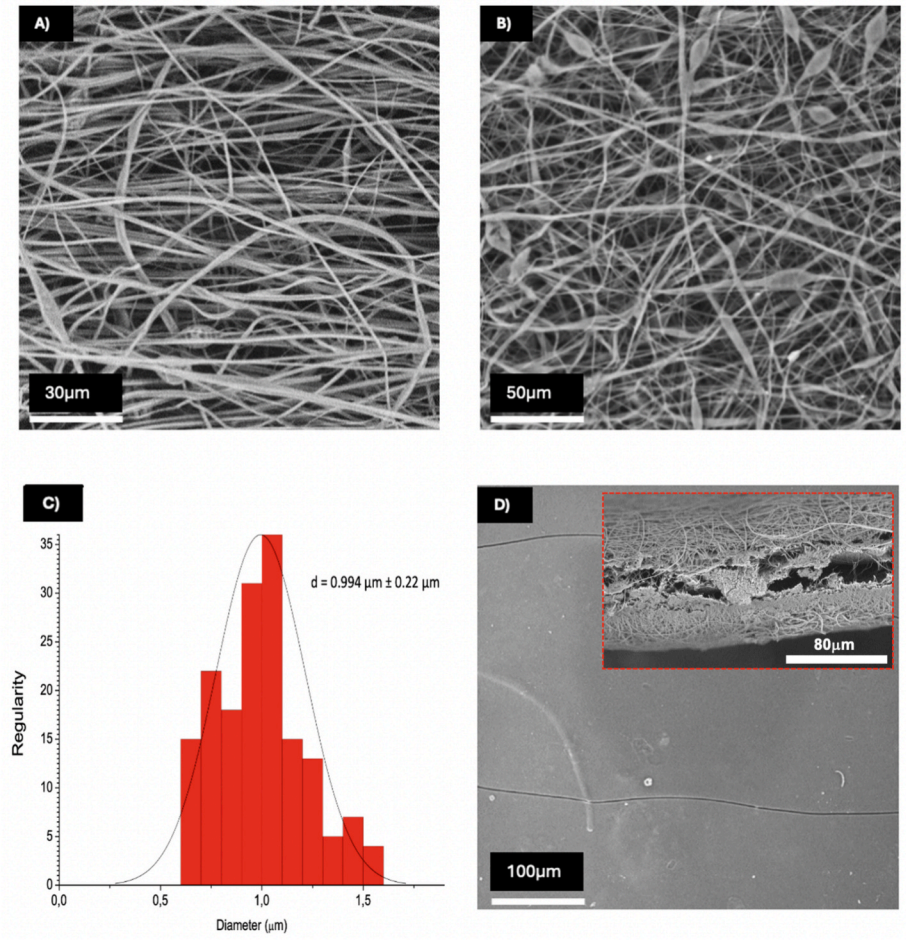

Fig. 1. SEM micrographs and fiber size distribution of the electrospun PLLA scaffold: A) PLLA nanofibers, B) plasma-treated PLLA nanofibers, C) size distribution of the PLLA nanofibers, and D) PLLA-AGMA1 nanocomposite (cross-section in the insert).

hydrogel.

3.2.2. *FTIR spectroscopy*

The spectrum of AGMA1 reported in Fig. 2A reveals several characteristic peaks due to the presence of the expected chemical residues for these oligomers. Specifically, a broad and pronounced peak in the range of 3400–3200 cm^{-1} can be observed, which is attributable to O=C-O–H and N–H groups. This suggests the presence of carboxyl and amine groups, consistent with the hypothesized structure. Moreover, an intense broad peak in the region of 1750–1620 cm^{-1} indicates the presence of carbonyl groups (C=O) due to amide groups and the carboxylic acid residue of BAC, coupled with conjugated double bonds (CH_2=CH_2-C=O) of the end chains. The ATR FTIR spectrum of the PLLA-AGMA1 composite (Fig. 2A) is mostly represented by several diagnostic peaks of AGMA1, suggesting that the PLLA-AGMA1 surface consists of the AGMA1 hydrogel. In addition, the decreased relative intensity of the 1620 cm^{-1} peak, attributable to acrylamide end groups, indicates successful radical crosslinking of AGMA1 oligomers, resulting in an interconnected hydrogel network.

3.2.3. *Contact angle measurements and sample wettability*

The contact angle measurements for samples PLLA, PLLA-NH_2, and PLLA-AGMA1 – recorded as 101°, 36°, ~0°, respectively – reveal significant differences in their surface wettability (Fig. 2B). The bare PLLA, with a contact angle of 101°, exhibits a hydrophobic surface, indicating limited water spreading and a high surface energy barrier for adhesion and proliferation. In contrast, the surface activated PLLA sample, with a contact angle of 36°, is endowed with a much more hydrophilic surface, allowing for greater water interaction at the cell/biomaterial interface. This behavior seems exacerbated in the PLLA-AGMA1 nanocomposite, with a total spreading of water, demonstrating complete wetting, which implies a highly hydrophilic nature likely due to an abundance of polar or charged groups in the AGMA1 hydrogel. These trends underscore how modifications in surface chemistry can critically influence wettability, a key factor in applications ranging from coatings to biomaterials for tissue engineering applications.

3.2.4. *Evaluation of the swelling degree and degradation kinetics*

The swelling degree of the PLLA-AGMA1 scaffold was evaluated in water, water at pH 4.0, and absolute ethanol. The latter conditions were specifically chosen to simulate the stresses encountered during the purification process (ethanol) and potential storage environments (pH 4.0). In particular, absolute ethanol was used to mimic the exposure to organic solvents typically employed in purification steps to extract water and byproducts, while acidic water reflects conditions relevant to storage pH. The sample exhibits a high swelling degree in aqueous environments (75–80 %) while maintaining excellent compactness (Fig. 2C). No statistically significant differences can be observed between ultrapure water and the acidic medium. In principle, a pH 4 can promote the ionization of amine groups in the composite, and the resulting electrostatic repulsion among these groups increases the absorption capacity by expanding the network structure to some extent [38]. This suggests that the potential increase in repulsion due to the cationic nature of the guanidinium and amine groups at pH 4 is effectively counteracted by the robust covalent interactions within the well-structured, rigid PLLA nanofiber network. The PLLA network plays a crucial role in limiting the

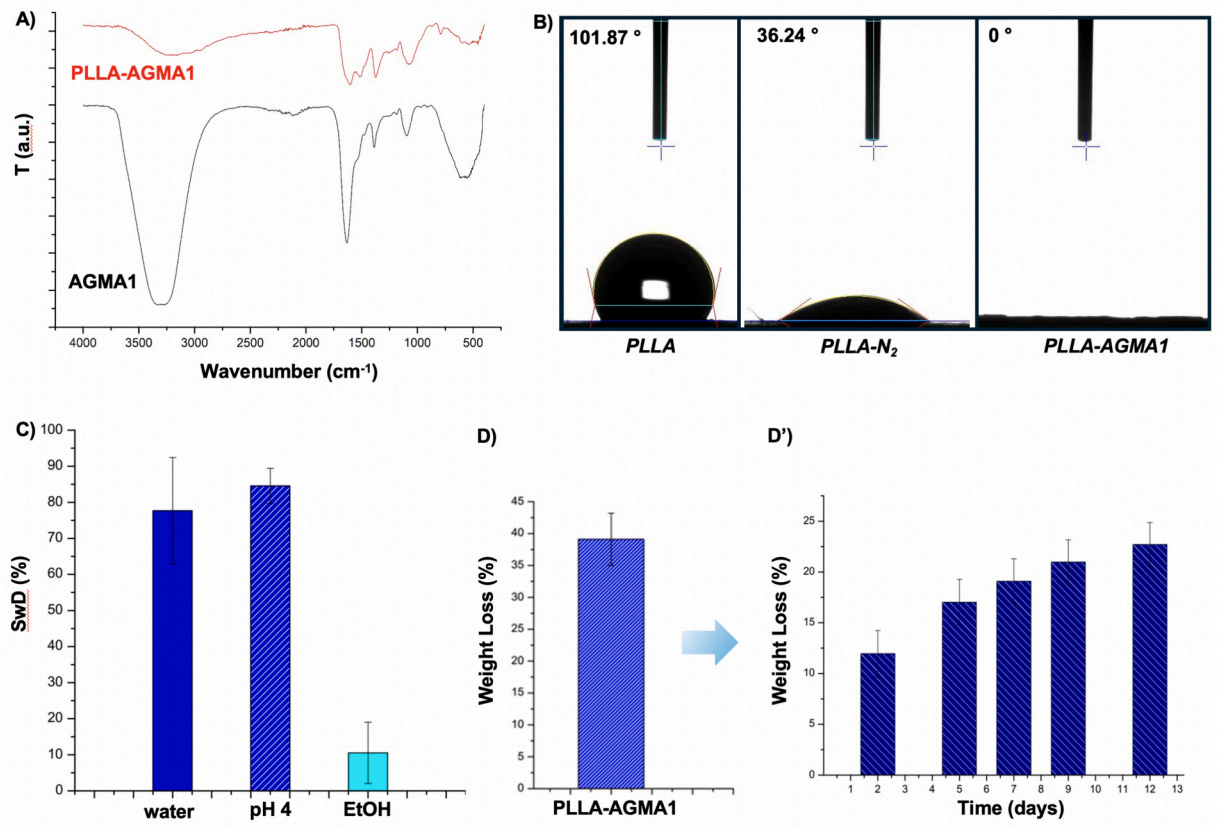

Fig. 2. A) FTIR spectra of AGMA1 and PLLA-AGMA1 samples. B) Contact angle values for dried PLLA, PLLA-NH_2, and PLLA-AGMA1 samples. C) Swelling degree (SwD) of the PLLA-AGMA1 sample in various media. D-D') Average degradation kinetics of the PLLA-AGMA1 nanocomposite in PBS pH 7.4.

swelling of the AGMA1 hydrogel, thereby preserving the scaffold's structural integrity under conditions that would otherwise promote enhanced swelling. This indirectly demonstrates that the hydrogel is chemically bonded to the electrospun scaffold. A previous preparation of the composite, performed without plasma treatment of the electrospun scaffold, and thus lacking a chemical bond between PLLA and AGMA1, resulted in the detachment and separation of the hydrogel component from the electrospun scaffold within 2–3 h of swelling in water (data not shown for brevity). A remarkable difference in the swelling degree of the composite can be observed in ethanol. The swelling degree in ethanol, significantly lower (less than 10 %), can be attributed to the poor affinity between the sample's surface, composed of AGMA1, and organic solvents. However, ethanol can be used to extract water and unreacted monomers during the reaction workup.

Two types of degradation tests were performed on the composites: i) a long-term test lasting four months (Fig. 2D) and another ii) monitoring the percentage of weight loss after 2, 5, 7, 9, and 12 days (Fig. 2D') at 37 °C in DMEM buffer at pH 7.4. The average weight loss of the composites is approximately 40 % w w^{-1} after 4 months of incubation under physiological conditions. Weight loss is primarily attributable to the degradation of the AGMA1 hydrogel component. This conclusion is also supported by the difference in degradation times between AGMA1 and PLLA, as the former degrades in vivo within three months, whereas PLLA is known to degrade much more slowly, maintaining its physical integrity for longer periods [22,39]. During the initial days of incubation, aligned with the cell adhesion tests discussed on the bottom, the composite PLLA-AGMA1 scaffold loses approximately 10 % of its weight after 2 days, increasing to about 25 % after 12 days. This indicates that the AGMA1 network degrades progressively during the adhesion and proliferation phases, potentially facilitating cell infiltration towards the scaffold nanofibers.

3.3. Thermo-mechanical characterizations

3.3.1. Thermal characterization

Thermogravimetric tests were performed in order to investigate the thermal degradation behavior of the electrospun PLLA, the composite and the bare AGMA1 hydrogel matrix. The thermogravimetric curves of the prepared samples, along with the corresponding derivative (DTG) curves, are presented in Fig. 3A-B, while the most significant results are reported in Table 1. As it is possible to observe, the thermal degradation of the electrospun PLLA occurs in one single step, showing a maximum degradation rate at 390 °C. The bare AGMA1 hydrogel exhibits a multi-step degradation, indicative of a complex decomposition mechanism attributed to the multifunctional nature of PAAs [40,41]. The initial significant weight loss at 117.7 °C corresponds to the water evaporation, while subsequent losses at 252.1, 316.6 and 431.0 °C are associated with PAAs degradation. These temperatures agree with values reported in the literature. The PAAs left a black and porous char residues (1.7 %), consistent with previously documented findings [40,41].

By comparing the degradation curve of the composite with those of its components, the thermal behavior appears more similar to that of the bare AGMA1 hydrogel matrix. The degradation steps occurring at temperatures above 200 °C (following the completion of water loss) align closely with those of the hydrogel. Moreover, the temperatures corresponding to the maximum degradation rate T_{1peak}, T_{2peak} and T_{3peak} are comparable to AGMA1 hydrogel but, in the case of T_{1peak} and T_{2peak}, are shifted to slightly higher temperatures. In the PLLA-AGMA1 composite, the degradation peak associated with PLLA is not observed. This is probably due to the overlap of this peak with those related to the degradation of the hydrogel. The composite also leaves a black, porous char residue (9.5 %). The higher m_{700} value with respect to the hydrogel is attributed to the lower water content in the PLLA-AGMA1 composite (water content of 30.3 % for PLLA-AGMA1 and 80.8 % for AGMA1

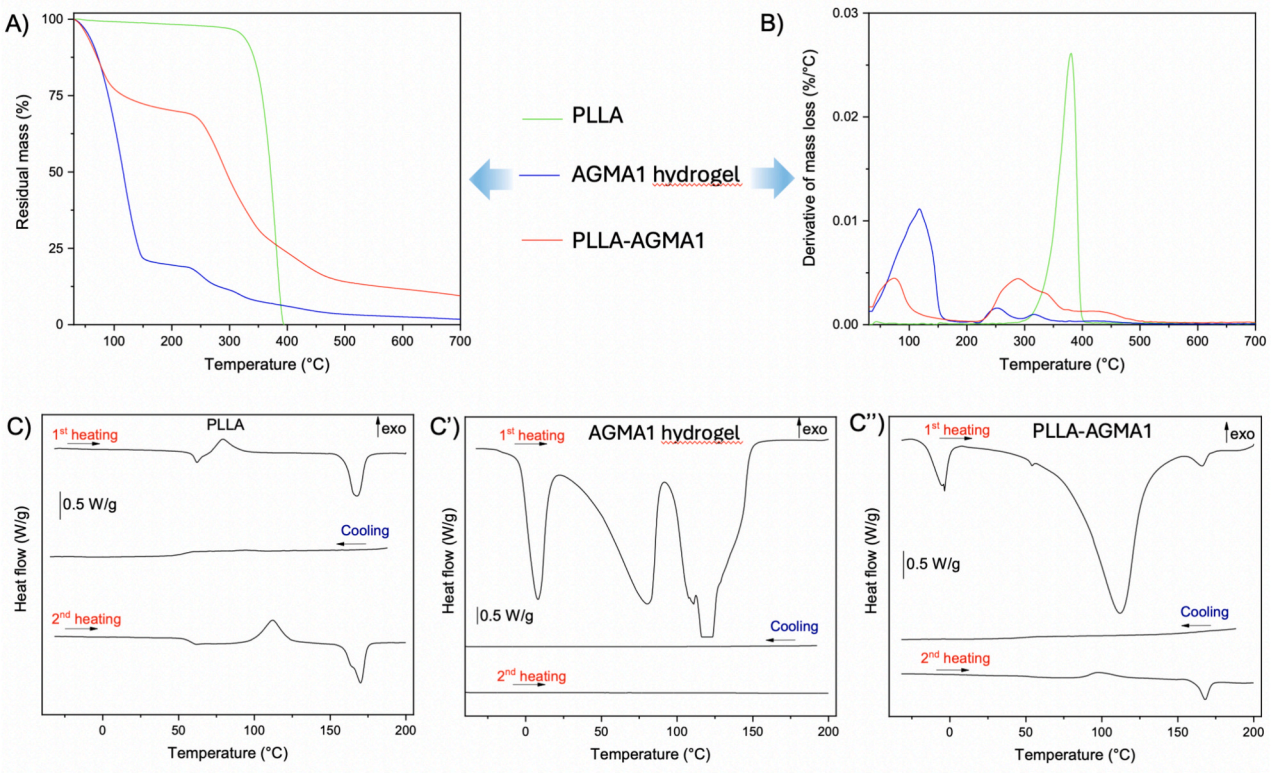

Fig. 3. TGA and DSC tests on PLLA, PLLA-AGMA1 and the plain AGMA1 hydrogel. Trends of (A) residual mass and (B) mass loss derivative as a function of temperature. DSC thermograms of (A) PLLA, (B) the AGMA1 hydrogel, and (C) the PLLA-AGMA1 composite.

Table 1
Results of the TGA tests on PLLA, PLLA-AGMA1 and the AGMA1 hydrogel.

Sample	$T_{5\%}$ (°C)	M_{200} (%)	M_{500} (%)	M_{700} (%)	$T_{H2O,\ peak}$ (°C)	$T_{PLLA,peak}$ (°C)	$T_{1,peak}$ (°C)	$T_{2,peak}$ (°C)	$T_{3,peak}$ (°C)
PLLA	320.8	97.8	0.0	0.0	–	389.9	–	–	–
AGMA1 hydrogel	55.2	19.2	3.8	1.7	117.7	–	252.1	316.6	431.0
PLLA-AGMA1	51.8	69.7	14.1	9.5	74.6	–	287.5	336.0	430.0

hydrogel). The DSC thermograms of the materials collected in the first heating scan, cooling scan and second heating scan are shown in Fig. 3C-C'', while the most important results are reported in Table 2.

By analyzing Fig. 3C, the DSC thermograms of the electrospun PLLA present the typical profile of semi-crystalline polymers. In the first heating scan, the glass transition temperature is 60.6 °C, the cold crystallization can be observed at 79.4 °C immediately after the glass transition, while the melting temperature is at 167.0 °C. The crystallinity degree is 32.4 %. Comparing the second heating scan to the first one, no significant differences are observed in the T_g and T_m values of PLLA. However, a notable difference lies in the cold crystallization temperature, which shifts to 111.9 °C. In the first heating scan, the proximity of the cold crystallization to the glass transition is likely attributable to the production process of the PLLA, as the electrospinning process may have facilitated the orientation of the macromolecules.

Consequently, the crystallization resumed immediately following the glass transition, driven by the enhanced mobility of the polymer chains. In the DSC traces of the bare AGMA1 hydrogel (Fig. 3C'), the first heating scan shows one narrow and two broad endothermic peaks. The narrow peak, centered around 0 °C, corresponds to the solid–liquid phase transition of water. The broader second peak, centered at approximately 70 °C and spanning a temperature range of 20 to 100 °C, is likely associated with water evaporation. The last peak centered at 130 °C may be attributed to a degradation step of the PAAs. This degradation is not visible in the TGA curves, probably due to an overlapping with the water loss. The second heating scan does not present any transitions. This is due to the loss of water during the first heating cycle and to the absence of thermal transition of PAAs in the temperature range considered. Finally, considering the thermal behavior of the PLLA-AGMA1 composite (Fig. 3C''), it is possible to identify the thermal transitions of both the AGMA1 hydrogel and PLLA. Differently from the hydrogel, in the temperature range 25–150 °C, only one endothermic peak is visible, probably the result of the overlapping of the two signals observed in the hydrogel. The glass transition and melting temperatures of PLLA in the composite are at slightly lower temperatures than those of the PLLA. For example, the T_g of PLLA-AGMA1 is 52.7 °C, compared to 60.6 °C for PLLA. As a final remark, the crystallinity of PLLA has not

Table 2
Results of the DSC tests on PLLA and PLLA-AGMA1.

Sample	T_g (°C)	T_{cc} (°C)	ΔH_{cc} (J/g)	T_m (°C)	ΔH_m (J/g)	X (%)
	1st heating					
PLLA	60.6	79.4	18.6	167.0	48.7	32.4
PLLA-AGMA1	52.7	–	–	165.6	–	–
	2nd heating					
PLLA	58.1	111.9	41.2	169.7	43.2	2.2
PLLA-AGMA1	53.3	97.3	–	167.5	–	–

been calculated since the exact PLLA weight content in the composite was unknown.

In Fig. 4A-A'', the trends of storage modulus, loss modulus, and loss tangent of PLLA and the PLLA-AGMA1 composite are shown as a function of temperature, while in Table 3 the most important results are reported. Analyzing Fig. 4A, the storage modulus of the materials differs, with the composite being stiffer compared to the electrospun PLLA. The impregnation with the AGMA1 hydrogel seems to promote a stiffening of the PLLA scaffold. As it was observed by SEM analysis, AGMA1 hydrogel entirely coated the electrospun fibers, saturating the meshes. The presence of the hydrogel probably reduces the mobility of the fibers, rendering the composite stiffer with respect to electrospun PLLA. The storage modulus evaluated at 37 °C (E'_{37}), which represents the working conditions, is reported in Table 3.

According to the literature, the stiffness of nerve tissue is around 38 MPa [42,43]. PLLA comes significantly closer to this value than the composite. However, the stiffness of PLLA-AGMA1 is relatively near, and such a minor stiffness difference might be appropriately addressed by tailoring the starting PLLA characteristics, understanding that the AGMA1 impregnation promotes stiffening of the starting material. The glass transition temperature of PLLA is evident in both materials within the temperature range of 65–75 °C. The peak of E'', associated with the glass transition of PLLA, has been detected at 67 °C in the electrospun PLLA and at 72 °C in the composite (Figure A'). The glass transition is also visible in the loss tangent plots at approx. 74 °C for both PLLA and PLLA-AGMA. An increase in the storage modulus is observed in both the composite and PLLA just above the glass transition. As already seen in DSC tests, this E' increase can be attributed to the cold crystallization, facilitated by the alignment of polymer chains along the direction of applied mechanical stress. In the case of the composite, the significant increase of E' before the glass transition phenomena could be associated with water loss [44].

3.3.2. Mechanical characterization

The representative stress–strain curves for the virgin and sutured PLLA electrospun mat and PLLA-AGMA composite are shown in Fig. 4B, while in Table 3 the mechanical properties are reported. Compared to the electrospun PLLA, the composite exhibits lower mechanical properties. In particular, moving from the PLLA-AGMA1 composite to PLLA results in a reduction of more than 50 % in both maximum stress and strain at break. However, the mechanical performance of the composite is extremely higher if compared with hydrogels (typically 0.05–0.2 MPa) [22]. On the other hand, both PLLA and PLLA-AGMA1 show lower tensile strength than that of peripheral nerve tissues (i.e., 4.9 to 30.4 MPa) [42,43]. The elastic modulus varies significantly, typically reported between 0.5 MPa and 2 MPa for neonatal nerves, indicating greater elasticity compared to adult nerves. The yield strength, or the point at which permanent damage occurs, is lower than in adult nerves and ranges from 0.5 MPa to 1.5 MPa. It might be noticed that the maximum tensile strength of decellularized peripheral nerves is comparable to that of PLLA-AGMA1 (0.6 vs 0.8 MPa, respectively) [45]. This suggests that the composite is suitable for peripheral nerve surgical intervention in PNI. As it could be expected, the suturing of two flaps of material, whether PLLA or PLLA-AGMA1 composite, worsens the mechanical resistance. This is likely due to the stress concentration in correspondence with the holes generated by the suturing operation.

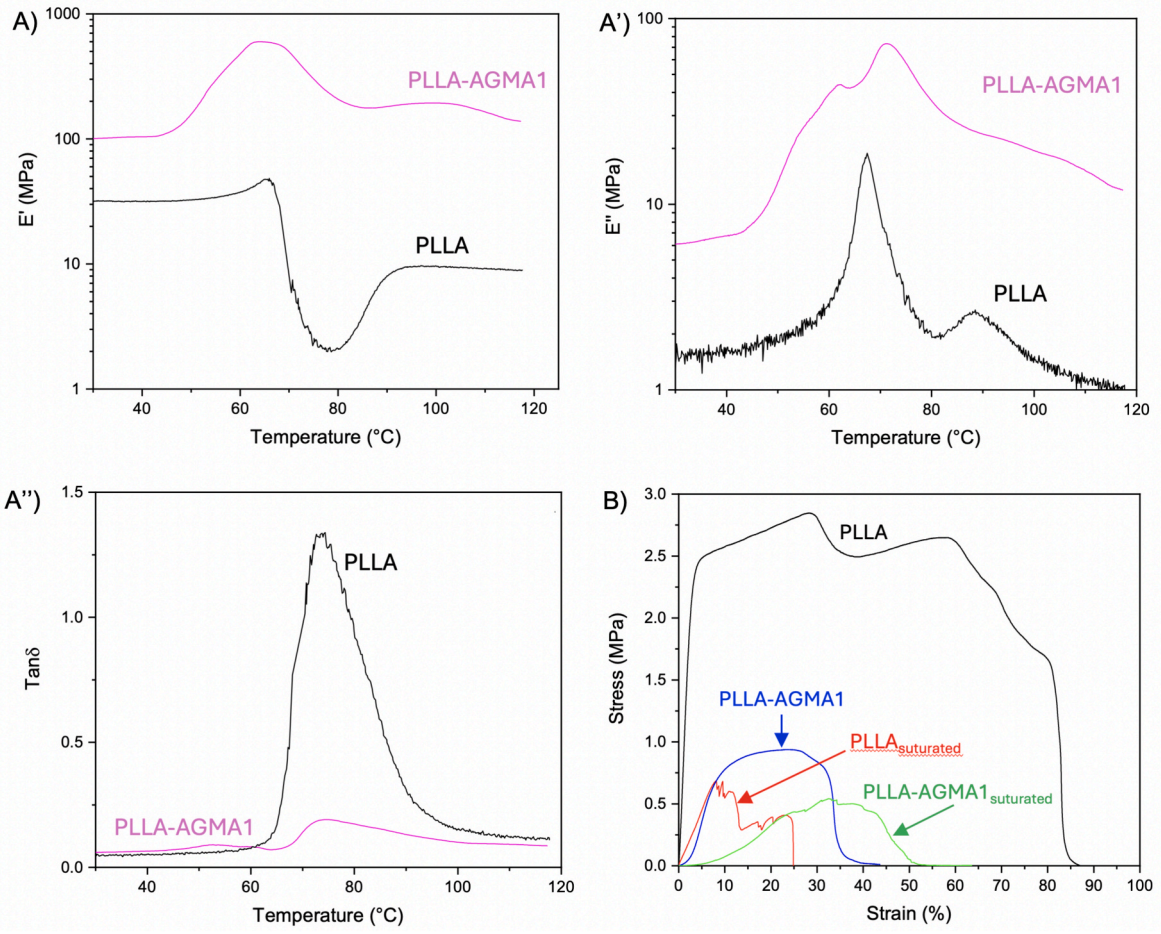

Fig. 4. Trends of storage modulus (A), loss modulus (A') and loss tangent (A'') as a function of the temperature from DMA tests on the PLLA and PLLA-AGMA1 samples. B) Representative stress–strain curves from quasi-static tensile tests on the PLLA and PLLA-AGMA1 samples (virgin and sutured).

Table 3
Results of the DMA tests and quasi-static tensile tests on PLLA and PLLA-AGMA1 samples (bare and sutured).

	E'_{37} (MPa)	E''_{peak1} (°C)	E''_{peak2} (°C)	$tan\delta_{peak}$	σ_{max} (MPa)	ε_{break} (%)
PLLA	31.7	67.4	88.4	73.8	2.7 ± 0.3	81.8 ± 4.6
PLLA$_{suturated}$	–	–	–	–	0.8 ± 0.5	23.2 ± 11.5
PLLA-AGMA1	103.5	73.1	–	73.7	0.8 ± 0.2	37.7 ± 4.2
PLLA-AGMA1s$_{uturated}$	–	–	–	–	0.4 ± 0.1	49.3 ± 10.8

The material plasticizes and fails in the section between the hole and the edges. This behavior is illustrated in Fig. 4B, where the progressive collapse is highlighted by the presence of drops and plateaus in the stress–strain curves, particularly for the sutured PLLA. As it can be noticed from Fig. 4B and Table 3, both the sutured PLLA and the composite exhibit lower maximum stress compared to their neat counterparts. Additionally, for PLLA, the strain at break is significantly reduced. The overall drop in mechanical performances of PLLA after the suturing operations is more significant than that displayed by PLLA-AGMA1. On the whole, the PLLA-AGMA1 composite shows a stable mechanical performance after applying sutures using the typical surgical approach used for nerve grafting.

3.4. Cell adhesion and proliferation assay

Human Schwann Cells (HSC) were cultured on PLLA/AGMA1 hydrogel scaffolds to evaluate their ability to sustain adhesion and proliferation, which is the first step of nerve regeneration. Indeed, it is a cornerstone of neurology that HSC stimulate axonal regeneration, promote the activation of mesenchymal precursors in surrounding tissues, create permissive channels for axonal growth, and release neurotrophic factors [46]. Moreover, it has been demonstrated that HSC incorporated into bioengineered scaffolds enhance nerve fiber migration and functionality. offering significant advancements in nerve regeneration [47]. These advancements include improved cell proliferation, increased production of neurotrophic factors, and support for axonal growth through their interaction with the scaffold. HSC adhesion and proliferation, expressed as percentage cell viability over time, were assessed on PLLA-AGMA1 scaffolds up to 9 days of incubation at 37 °C. Cell viability data, calculated with respect to HSC proliferated in untreated wells, indicate that at 1- and 2-days post-seeding, cell viability is significantly higher in the control group compared to the scaffold group (75–80 % vs 100 %) (Fig. 5).

After 5 days of incubation, the alamarBlue assay reveals that HSC proliferate faster in the PLLA-AGMA1 scaffold, reaching a plateau up to 9 days of incubation. In detail, the composite group demonstrates superior cell viability relative to the control (120–110 % vs 100 %), mainly due to the 3D network of PLLA-AGMA1 which extensively support proliferation of infiltrated cells due to partial AGMA1 surface degradation (17 % w w^{-1} after 5 days, Fig. 2D'). The relationship between

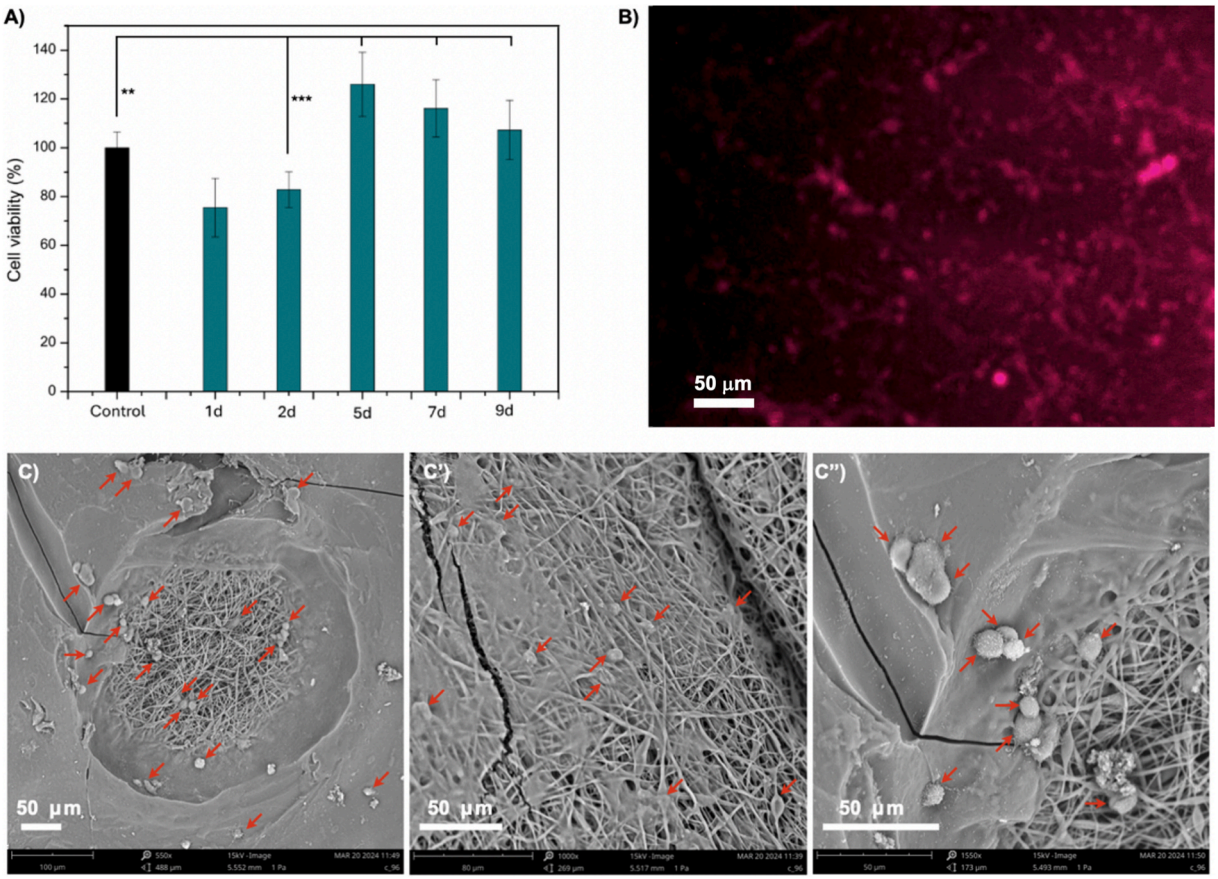

Fig. 5. (A) Human Schwann cell (HSC) viability on PLLA-AGMA1 scaffolds after 9 days incubation at 37 °C. (B) Fluorescence micrograph of HSC stained with CellTracker Deep Red after 5 days of incubation on PLLA-AGMA1 scaffolds: magnification 5x. (C-C''') Scanning electron micrographs of PLLA-AGMA1 scaffolds incubated with HSC for 5 days.

degradation kinetics and cell viability is clearly visible in Fig. 2D', which indicate a continuous increase in weight loss of the sample, reaching approximately 23 % weight loss in twelve days. This suggests a correlation between reduced cell growth and hydrogel degradation. During the first two days of degradation, more than 50 % of the total weight loss occurs. These findings suggest that the majority part of the degradation of the hydrogel on the surface occurs within approximately one week, reaching about 19 % of weight loss, that is the 83 % of the total weight loss. The moderate decline in cell viability from 5 to 9 days observed in the composite indicates that the scaffold provides, despite the loss of the hydrogel matrix, a more stable environment for long-term cell survival. The huge presence of HSC in the PLLA-AGMA1 after 5 days of incubation is demonstrated also by fluorescence microscopy and SEM analyses reported in Fig. 5B and 5C-C'', respectively. SEM analysis was performed at 5 days post-seeding, as it represents a stage where HSC exhibit meaningful adhesion and spreading. At earlier time points cells typically tend to detach during sample processing due to insufficient anchorage, particularly when freeze-drying is involved. By day 9, although cell viability remains high, HSC predominantly migrate toward the scaffold's interior, particularly within regions enriched in AGMA1 hydrogel. This limits surface-level SEM imaging due to reduced cell presence on the outer layers (data not shown). In particular, SEM micrographs also show the partial degradation of the AGMA1 matrix yielding craters with exposed porous nanofibers which allow HSC infiltration throughout the saffold. This behavior, in addition to the other above discussed results, suggests that the composite could be potentially utilized as an implantable biodegradable scaffold to support the role of HSC in promoting axonal regeneration and enhancing neural repair outcomes.

4. Conclusions

Here, a biodegradable composite hydrogel endowed with high stiffness, suturability, and the ability to promote adhesion and proliferation of human Schwann cells was developed and studied. The composite hydrogel, named PLLA-AGMA1, was prepared using a nitrogen plasma activated PLLA electrospun scaffold, selected for their porosity, mechanical robustness, and biodegradability, embedded in a biomimetic poly(amidoamine) hydrogel matrix (AGMA1) with RGD-like structure, able to promote cell adhesion and proliferation. The composite hydrogel scaffold PLLA-AGMA1 was obtained by simply activating PLLA nanofibers with primary amines by nitrogen plasma, and by conjugating these Michael donor functions with acrylamide end-capped AGMA1 oligomers obtained by polyaddition of agmatine and excess bisacrylamide, followed by UV light crosslinking of double bonds. The soft and porous matrix of the AGMA1 hydrogel component supported cell adhesion and growth via RGD residues, while the electrospun PLLA mats provided mechanical stability indicative of the stiffness of the native ECM and allowed cell elongation. Morphological analysis confirmed the integrity of the material since nanofiber diameters were homogeneous, with a diameter of 0.99 ± 0.22 μm, a uniform hydrogel coating, and good swelling properties in aqueous environments. Notwithstanding the high swelling degree in water (80 %), the composite hydrogel showed a stiff elastic response and stable mechanical properties up to high levels of stress, which may indicate a strong internal network. The biological tests performed using human Schwann cells showed the potential of this scaffold for cell adhesion, proliferation, and long-term vitality (up to 9 days). The adhesion studies, compared to those on hydrogel degradation, have shown how it is likely that during cell culture the hydrogel degrades, and PLLA portion remains, offering a stable 3-D matrix that can support cell culture while also providing structural reinforcement and continuity to facilitate nerve reparation. Undoubtedly, further in-depth and extended experiments will be required to thoroughly evaluate PLLA-AGMA1 composite as potential material for biomedical uses, particularly in vivo study as implantable and regenerative material. However, the observed properties made the PLLA-AGMA1 composite a very promising implantable device usable in peripheral nerve regeneration and implantation as a bioengineered material with Schwann cells encapsulated within the hydrogel phase.

CRediT authorship contribution statement

Sergio Sciré: Methodology, Formal analysis, Writing – review & editing, Writing – original draft, Investigation, Data curation. **Marica Bianchi:** Methodology, Writing – original draft, Investigation, Formal analysis, Data curation. **Marco Pensabene:** Writing – original draft, Methodology, Data curation, Investigation. **Andrea Dorigato:** Writing – review & editing, Writing – original draft, Supervision, Methodology, Funding acquisition, Formal analysis, Data curation, Resources, Investigation. **Nicolò Mauro:** Writing – review & editing, Writing – original draft, Supervision, Resources, Project administration, Methodology, Investigation, Funding acquisition, Formal analysis, Conceptualization.

Declaration of competing interest

The authors declare that they have no known competing financial interests or personal relationships that could have appeared to influence the work reported in this paper.

Acknowledgements

S.S. thanks SiciliAn MicronanOTecH Research And Innovation CEnter "SAMOTHRACE" (MUR, PNRR-M4C2, ECS_00000022), spoke 3 - Universita ' degli Studi di Palermo S2-COMMs - Micro and Nanotechnologies for Smart & Sustainable Communities, for funding.

The authors thank the Advanced Technologies Network Center (ATeN Center) of the University of Palermo- Laboratory of Preparation and Analysis of Biomaterials, for the contact angle measurements, scansion electron microscopy micrographs, and electrospinning facility access.

Data availability

No data was used for the research described in the article.

References

[1] T. Wan, F.S. Zhang, M.Y. Qin, H.R. Jiang, M. Zhang, Y. Qu, Y.L. Wang, P.X. Zhang, Growth factors: bioactive macromolecular drugs for peripheral nerve injury treatment – molecular mechanisms and delivery platforms, Biomed. Pharmacother. 170 (2024), https://doi.org/10.1016/j.biopha.2023.116024.

[2] G.P. Watchmaker, S.E. Mackinnon, Advances in peripheral nerve repair, Clin. Plast. Surg. 24 (1) (1997) 63–73, https://doi.org/10.1016/S0094-1298(20)32583-9.

[3] X. Yao, T. Xue, B. Chen, X. Zhou, Y. Ji, Z. Gao, B. Liu, J. Yang, Y. Shen, H. Sun, X. Gu, B. Dai, Advances in biomaterial-based tissue engineering for peripheral nerve injury repair, Bioact. Mater. 46 (2025) 150–172, https://doi.org/10.1016/J.BIOACTMAT.2024.12.005.

[4] N. Rbia, A.Y. Shin, The role of nerve graft substitutes in motor and mixed motor/sensory peripheral nerve injuries, J. Hand Surg. Am. 42 (5) (2017) 367–377, https://doi.org/10.1016/J.JHSA.2017.02.017.

[5] S.P. Garg, A.M. Hassan, A. Patel, S. Ketheeswaran, R.D. Galiano, J.H. Ko, A systematic review of nerve grafting, end-to-end repair, and nerve transfer for obturator nerve injuries, Int. J. Gynecol. Cancer 32 (9) (2022) 1177–1182, https://doi.org/10.1136/IJGC-2022-003565.

[6] A. Muheremu, A.Q. Past, Present, and future of nerve conduits in the treatment of peripheral nerve injury, Biomed Res. Int. (2015), https://doi.org/10.1155/2015/237507.

[7] Z. Sun, D. Zhu, H. Zhao, J. Liu, P. He, X. Luan, H. Hu, X. Zhang, G. Wei, Y. Xi, Recent advance in bioactive hydrogels for repairing spinal cord injury: material design, biofunctional regulation, and applications, J Nanobiotechnology 21 (1) (2023), https://doi.org/10.1186/s12951-023-01996-y.

[8] Z. Sun, H. Hu, X. Zhang, X. Luan, Y. Xi, G. Wei, X. Zhang, Recent advances in peptide-based bioactive hydrogels for nerve repair and regeneration: from material design to fabrication, functional tailoring and applications, J. Mater. Chem. B 12 (9) (2024) 2253–2273, https://doi.org/10.1039/D4TB00019F.

[9] M. Rossi, I. Rana, P.S. Buonuomo, G. Battafarano, E. Mariani, M. D'Agostini, O. Porzio, V. De Martino, S. Minisola, M. Macchiaiolo, R. De Vito, D. Vecchio, M. V. Gonfiantini, A. Jenkner, A. Bartuli, A. Del Fattore, Dysregulated MiRNAs in bone cells of patients with gorham-stout disease, FASEB J. 35 (3) (2021), https://doi.org/10.1096/FJ.202001904RR.

[10] X. Gu, F. Ding, Y. Yang, J. Liu, Construction of tissue engineered nerve grafts and their application in peripheral nerve regeneration, Prog. Neurobiol. 93 (2) (2011) 204–230, https://doi.org/10.1016/J.PNEUROBIO.2010.11.002.

[11] Samadian, H.; Ehterami, A.; … A. S.-I. journal of; 2020, undefined. Sophisticated Polycaprolactone/Gelatin Nanofibrous Nerve Guided Conduit Containing Platelet-Rich Plasma and Citicoline for Peripheral Nerve Regeneration: In Vitro And. *ElsevierH Samadian, A Ehterami, A Sarrafzadeh, H Khastar, M Nikbakht, A Rezaei, L CheginiInternational journal of biological macromolecules, 2020•Elsevier*.

[12] Matsumine, H.; Sasaki, R.; Yamato, M.; Okano, T.; Sakurai, H. A Polylactic Acid Non-woven Nerve Conduit for Facial Nerve Regeneration in Rats. *Wiley Online LibraryH Matsumine, R Sasaki, M Yamato, T Okano, H SakuraiJournal of Tissue Engineering and Regenerative Medicine, 2014•Wiley Online Library* **2012**, *8* (6), 454–462. doi: 10.1002/term.1540.

[13] Stocco, E.; Barbon, S.; Faccio, D.; Petrelli, L.; Bio, D. I.-M. T.; 2023, undefined. Development and Preclinical Evaluation of Bioactive Nerve Conduits for Peripheral Nerve Regeneration: A Comparative Study. *ElsevierE Stocco, S Barbon, D Faccio, L Petrelli, D Incendi, A Zamuner, E De Rose, M ConfalonieriMaterials Today Bio, 2023•Elsevier*.

[14] W.H. Chooi, S.Y. Chew, Modulation of cell-cell interactions for neural tissue engineering: potential therapeutic applications of cell adhesion molecules in nerve regeneration, Biomaterials 197 (2019) 327–344, https://doi.org/10.1016/J.BIOMATERIALS.2019.01.030.

[15] J.B. McCarthy, A.P.N. Skubitz, Q. Zhao, X.Y. Yi, D.J. Mickelson, D.J. Klein, L. T. Furcht, RGD-independent cell adhesion to the carboxy-terminal heparin-binding fragment of fibronectin involves heparin-dependent and -independent activities, J. Cell Biol. 110 (3) (1990) 777–787, https://doi.org/10.1083/jcb.110.3.777.

[16] M.D. Pierschbacher, E. Ruoslahti, Cell attachment activity of fibronectin can be duplicated by small synthetic fragments of the molecule, Nature 309 (5963) (1984) 30–33, https://doi.org/10.1038/309030A0.

[17] X. Liu, J. Jiang, H. Liu, F. Liu, H. Shao, S. Chen, S. Wu, Adjusting morphology, structure, and mechanical properties of electrospun high-molecular-weight poly(l-Lactic-Acid) Nanofibrous yarns through hot stretching treatment, Macromol. Biosci. 25 (5) (2025) 2400656, https://doi.org/10.1002/MABI.202400656;PAGE:STRING:ARTICLE/CHAPTER.

[18] J. Pan, Q. Meng, L. Zhang, C. Zhang, S. Wu, H. Zhai, Electrospun amine-modified polysuccinimide/polycaprolactone nanofiber hydrogel dressings as antibacterial and hemostatic wound dressing applications, Colloids Surf. B Biointerfaces 252 (2025), https://doi.org/10.1016/j.colsurfb.2025.114648.

[19] P. Ferruti, S. Bianchi, E. Ranucci, F. Chiellini, V. Caruso, Novel poly(Amido-Amine)-based hydrogels as scaffolds for tissue engineering, Macromol. Biosci. 5 (7) (2005) 613–622, https://doi.org/10.1002/MABI.200500020.

[20] N. Mauro, A. Manfredi, E. Ranucci, P. Procacci, M. Laus, D. Antonioli, C. Mantovani, V. Magnaghi, P. Ferruti, Degradable poly(Amidoamine) hydrogels as scaffolds for in vitro culturing of peripheral nervous system cells, Macromol. Biosci. 13 (3) (2013) 332–347, https://doi.org/10.1002/mabi.201200354.

[21] N. Mauro, F. Chiellini, C. Bartoli, M. Gazzarri, M. Laus, D. Antonioli, P. Griffiths, A. Manfredi, E. Ranucci, P. Ferruti, RGD-mimic polyamidoamine-montmorillonite composites with tunable stiffness as scaffolds for bone tissue-engineering applications, J. Tissue Eng. Regen. Med. (2016), https://doi.org/10.1002/term.2115.

[22] C. Gualandi, N. Bloise, N. Mauro, P. Ferruti, A. Manfredi, M. Sampaolesi, A. Liguori, R. Laurita, M. Gherardi, V. Colombo, L. Visai, M.L. Focarete, E. Ranucci, Poly-l-lactic acid nanofiber-polyamidoamine hydrogel composites: preparation, properties, and preliminary evaluation as scaffolds for human pluripotent stem cell culturing, Macromol. Biosci. 16 (10) (2016) 1533–1544, https://doi.org/10.1002/mabi.201600061.

[23] J. Franchini, E. Ranucci, P. Ferruti, M. Rossi, R. Cavalli, Synthesis, physicochemical properties, and preliminary biological characterizations of a novel amphoteric agmatine-based Poly(Amidoamine) with RGD-like repeating units, Biomacromolecules 7 (4) (2006) 1215–1222, https://doi.org/10.1021/BM060054M.

[24] S. Liu, S. Qin, M. He, D. Zhou, Q. Qin, H. Wang, Current applications of poly(Lactic Acid) composites in tissue engineering and drug delivery, Compos. B Eng. 199 (2020) 108238, https://doi.org/10.1016/J.COMPOSITESB.2020.108238.

[25] J. Zan, G. Qian, F. Deng, J. Zhang, Z. Zeng, S. Peng, C. Shuai, Dilemma and breakthrough of biodegradable poly-l-lactic acid in bone tissue repair, J. Mater. Res. Technol. 17 (2022) 2369–2387, https://doi.org/10.1016/J.JMRT.2022.01.164.

[26] R. Li, Y. Ma, Y. Zhang, M. Zhang, D. Sun, Potential of RhBMP-2 and dexamethasone-loaded Zein/PLLA scaffolds for enhanced in vitro osteogenesis of mesenchymal stem cells, Colloids Surf. B Biointerfaces 169 (2018) 384–394, https://doi.org/10.1016/J.COLSURFB.2018.05.039.

[27] H. Xu, Z. Fan, The role and mechanism of schwann cells in the repair of peripheral nerve injury, Cell Tissue Res. (2025), https://doi.org/10.1007/S00441-025-03957-3.

[28] U. Namgung, The role of schwann cell-axon interaction in peripheral nerve regeneration, Cells Tissues Organs 200 (1) (2014) 6–12, https://doi.org/10.1159/000370324.

[29] C.A. Webber, K.J. Christie, C. Cheng, J.A. Martinez, B. Singh, V. Singh, D. Thomas, D.W. Zochodne, Schwann cells direct peripheral nerve regeneration through the netrin-1 receptors, DCC and Unc5H2, Glia 59 (10) (2011) 1503–1517, https://doi.org/10.1002/GLIA.21194.

[30] T. Zheng, L. Wu, S. Sun, J. Xu, Q. Han, Y. Liu, R. Wu, G. Li, Co-culture of schwann cells and endothelial cells for synergistically regulating dorsal root ganglion behavior on chitosan-based anisotropic topology for peripheral nerve regeneration, Burns Trauma 10 (2022) 30, https://doi.org/10.1093/BURNST/TKAC030.

[31] P. Ferruti, N. Mauro, A. Manfredi, E. Ranucci, Hetero-difunctional dimers as building blocks for the synthesis of poly(Amidoamine)s with hetero-difunctional chain terminals and their derivatives, J. Polym. Sci. A Polym. Chem. 50 (23) (2012) 4947–4957, https://doi.org/10.1002/POLA.26325.

[32] P.C. Griffiths, N. Mauro, D.M. Murphy, E. Carter, S.C.W. Richardson, P. Dyer, P. Ferruti, Self-assembled PAA-based nanoparticles as potential gene and protein delivery systems, Macromol. Biosci. 13 (5) (2013), https://doi.org/10.1002/mabi.201200462.

[33] P. Ferruti, J. Franchini, M. Bencini, E. Ranucci, G.P. Zara, L. Serpe, L. Primo, R. Cavalli, Prevailingly cationic agmatine-based amphoteric polyamidoamine as a nontoxic, nonhemolytic, and "Stealthlike" DNA complexing agent and transfection promoter, Biomacromolecules 8 (5) (2007) 1498–1504, https://doi.org/10.1021/bm061126c.

[34] P. Ferruti, Poly(Amidoamine)s: past, present, and perspectives, J. Polym. Sci. A Polym. Chem. 51 (11) (2013) 2319–2353, https://doi.org/10.1002/POLA.26632.

[35] E. Ranucci, P. Ferruti, E. Lattanzio, A. Manfredi, M. Rossi, P.R. Mussini, F. Chiellini, C. Bartoli, Acid-base properties of poly(Amidoamine)s, J. Polym. Sci. A Polym. Chem. 47 (24) (2009) 6977–6991, https://doi.org/10.1002/POLA.23737.

[36] N. Mauro, C. Fiorica, M. Giuffrè, C. Calà, C.M. Maida, G. Giammona, A self-sterilizing fluorescent nanocomposite as versatile material with broad-spectrum antibiofilm features, Mater. Sci. Eng. C 117 (2020), https://doi.org/10.1016/J.MSEC.2020.111308.

[37] N. Mauro, C. Scialabba, G. Pitarresi, G. Giammona, Enhanced adhesion and in situ photothermal ablation of cancer cells in surface-functionalized electrospun microfiber scaffold with graphene oxide, Int. J. Pharm. 526 (1–2) (2017), https://doi.org/10.1016/j.ijpharm.2017.04.045.

[38] N. Vishal Gupta, H.G. Shivakumar, Investigation of swelling behavior and mechanical properties of a PH-sensitive superporous hydrogel composite, Iran J Pharm Res 11 (2) (2012) 481.

[39] N. Mauro, M. Andrea Utzeri, A. Sciortino, M. Cannas, F. Messina, G. Cavallaro, G. Giammona, Printable thermo- and photo-stable poly(D,L-Lactide)/carbon nanodots nanocomposites via heterophase melt-extrusion transesterification, Chem. Eng. J. 443 (2022) 136525, https://doi.org/10.1016/J.CEJ.2022.136525.

[40] A. Beduini, F. Carosio, P. Ferruti, E. Ranucci, J. Alongi, Polyamidoamines derived from natural α-amino acids as effective flame retardants for cotton, Polymers (Basel) 13 (21) (2021) 3714, https://doi.org/10.3390/polym13213714.

[41] A. Manfredi, F. Carosio, P. Ferruti, E. Ranucci, J. Alongi, Linear polyamidoamines as novel biocompatible phosphorus-free surface-confined intumescent flame retardants for cotton fabrics, Polym. Degrad. Stab. 151 (2018) 52–64, https://doi.org/10.1016/j.polymdegradstab.2018.02.020.

[42] V. Orozco, R. Magee, S. Balasubramanian, A. Singh, A systematic review of the tensile biomechanical properties of the neonatal brachial plexus, J. Biomech. Eng. 143 (11) (2021), https://doi.org/10.1115/1.4051399.

[43] L. Yan, A. Entezari, Z. Zhang, J. Zhong, J. Liang, Q. Li, J. Qi, An Experimental and numerical study of the microstructural and biomechanical properties of human peripheral nerve endoneurium for the design of tissue scaffolds, Front. Bioeng. Biotechnol. 10 (2022), https://doi.org/10.3389/fbioe.2022.1029416.

[44] A. Karydis-Messinis, D. Moschovas, M. Markou, K. Tsirka, C. Gioti, E. Bagli, C. Murphy, A.E. Giannakas, A. Paipetis, M.A. Karakassides, A. Avgeropoulos, C. E. Salmas, N.E. Zafeiropoulos, Hydrogel membranes from chitosan-fish Gelatin-glycerol for biomedical applications: chondroitin sulfate incorporation effect in membrane properties, Gels 9 (11) (2023) 844, https://doi.org/10.3390/gels9110844.

[45] G.H. Borschel, K.F. Kia, W.M. Kuzon, R.G. Dennis, Mechanical properties of acellular peripheral nerve, J. Surg. Res. 114 (2) (2003) 133–139, https://doi.org/10.1016/S0022-4804(03)00255-5.

[46] M.J. Carr, A.P. Johnston, Schwann cells as drivers of tissue repair and regeneration, Curr. Opin. Neurobiol. 47 (2017) 52–57, https://doi.org/10.1016/j.conb.2017.09.003.

[47] Y. Al-Hadeethi, A. Nagarajan, S. Hanuman, H. Mohammed, A.M. Vetekar, G. Thakur, L.N.M. Dinh, Y. Yao, E.M. Mkawi, M.A. Hussein, V. Agarwal, M. Nune, Schwann cell-matrix coated PCL-MWCNT multifunctional nanofibrous scaffolds for neural regeneration, RSC Adv. 13 (2) (2023) 1392–1401, https://doi.org/10.1039/D2RA05368C.